Hybrid Biodegradable Nanomotors through Compartmentalized Synthesis

Imke A. B. Pijpers,[a] Shoupeng Cao,[a] Antoni Llopis-Lorente,[a] Jianzhi Zhu,[a] Shidong Song,[a] Rick R. M. Joosten,[b] Fenghua Meng,[c] Heiner Friedrich,[b,d] David S. Williams,[e] Samuel Sánchez,[f] Jan C. M. van Hest,*[a] and Loai K. E. A. Abdelmohsen*[a]

[a] I. A. B. Pijpers, S. Cao, Dr. A. Llopis-Lorente, J. Zhu, S. Song, Prof. J. C. M. van Hest, Dr. L. K. E. A. Abdelmohsen**
Department of Bio-Organic Chemistry,
Institute of Complex Molecular Systems (ICMS), Eindhoven University of Technology,
Het Kranenveld 14, 5600 MB Eindhoven, The Netherlands
**E-mail: j.c.m.v.hest@tue.nl, l.k.e.a.abdelmohsen@tue.nl*

[b] R. R. M. Joosten, Dr. H. Friedrich
Center for Multiscale Electron Microscopy (CMEM)
Eindhoven University of Technology,
Het Kranenveld 14, 5600 MB Eindhoven, The Netherlands

[c] Prof. F. Meng
Biomedical Polymers Laboratory, College of Chemistry,
Chemical Engineering and Materials Science, Soochow University,
Suzhou 215123, PR China

[d] Dr. H. Friedrich
Department of Chemical Engineering and Chemistry, Physical Chemistry,
Institute of Complex Molecular Systems (ICMS), Eindhoven University of Technology,
Het Kranenveld 14, 5600 MB Eindhoven, The Netherlands

[e] Dr. D.S. Williams
Department of Chemistry, College of Science
Swansea University
Swansea SA2 8PP, UK

[f] Prof. S. Sánchez
Institute for Bioengineering of Catalonia (IBEC)
The Barcelona Institute of Science and Technology
Baldiri i Reixac 10-12, 08028 Barcelona, Spain

* To whom correspondence should be addressed, email: l.k.e.a.abdelmohsen@tue.nl; j.c.m.v.hest@tue.nl

S1. Experimental Procedures

Materials

All chemicals were used as received unless stated otherwise. Poly(ethylene glycol) 1K and 2K were purchased from JenKem technology and freeze-dried before use. D,L-lactide was purchased from Acros Organics. Sulfo-Cyanine5 NHS ester was purchased from Lumiprobe. Bovine Serum Albumin (BSA), potassium permanganate, hydrogen peroxide (37% solution) and sodium thiosulfate pentahydrate were supplied by Sigma Aldrich. Fiducial Gold markers (20 nm) were purchased from CMC Utrecht. Ultra-pure water (18.2 MΩ) was obtained from Merck Millipore Q-Pod system with a 0.22 µm Millipore ® Express 40 filter. Dialysis Membranes (MWCO 12-14000 g mol-1 Spectra/Por®) were supplied by VWR and used for dialysis. Sodium chloride was purchased from Merck. Trypsin-EDTA, Penicillin streptomycin, no mycoplasma fetal bovine serum (FBS), Dulbecco's Modified Eagle Medium (DMEM), phosphate buffered saline (PBS), Hoechst 33342, CM-H2DCF were purchased from ThermoFisher Scientific.

Instrumentation

Nuclear Magnetic Resonance (NMR): Proton nuclear magnetic resonance measurements were performed on a Bruker 400 Ultrashield spectrometer equipped with a Bruker SampleCase autosampler, using $CDCl_3$ as a solvent and TMS as internal standard.

Gel permeation chromatography (GPC): GPC was conducted using a Shimadzu Prominence-i GPC system with a PL gel 5 µm mixed D and mixed C column (Polymer Laboratories) with PS standard and equipped with a Shimadzu RID-20A differential refractive index detector. THF was used as an eluent with a flow rate of 1 mL min^{-1}.

Dynamic Light Scattering (DLS): DLS measurements were performed on a Malvern instrument Zetasizer (model Nano ZSP) equipped with an autosampler. Zetasizer software was used to process and analyze the data. All samples were prepared by diluting them 10-fold in ultrapure water and measurements were carried out in standard disposable cuvettes.

Nanotracking Analysis (NTA): Nanosight Tracking Analysis was carried out on a Nanosight NS300 equipped with a blue laser (488 nm) and sCMOS camera. Samples were prepared by diluting them 1000-fold in either ultrapure water or PBS.

Cryogenic transmission electron microscopy (cryo-TEM): Experiments were performed using the TU/e CryoTitan (Thermo Fisher Scientific) equipped with a field emission gun and autoloader and operated at 300 kV acceleration voltage in low-dose bright-field TEM mode. Samples for cryo-TEM were prepared by glow-discharging the grids (Lacey carbon coated, R2/2, Cu, 200 mesh, EM sciences) in a Cressington 208 carbon coater for 40 seconds. Then, 4 µl of the polymersome solution was pipetted on the grid and blotted in a Vitrobot MARK III at room temperature and 100% humidity. The grid was blotted for 3 seconds (offset -3) and directly plunged and frozen in liquid ethane. Cryo-TEM images were acquired with zero loss energy filtering mode (Gatan GIF 2002, 20eV energy slit) on a CCD camera (Gatan model 794).

Microplate reader: Cell viability by a standard 3-(4,5-dimethylthiazol-2-yl)-2,5-diphenyl tetrazolium bromide (MTT) assay and fluorescence was measured on a TECAN Safire2 platereader.

Confocal microscopy imaging: Confocal microscopy was performed using a Leica TCS 264 SP5X system.

S2. Procedures

Synthesis of poly(ethylene)glycol-b-poly(D,L-lactide)

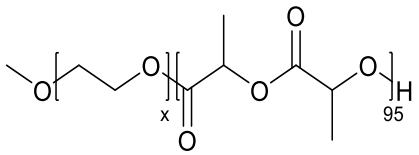

The reaction was carried out using previously published procedures.[1,2] Briefly, poly(ethylene) glycol (PEG) was weighed into a flame-dried 50 mL round bottom flask. D,L-lactide (DLLA, 95 eq.) was added and all reagents were subsequently dried by co-evaporation with toluene. Thereafter, dry dichloromethane (DCM) was added (so that the [monomer] = 0.5M) under Argon. Afterwards, 1,8-diazo-bicyclo[5.4.0]undec-7-ene (DBU, 0.5 eq to PEG) was added to initiate the ring opening polymerization. The reaction was left stirring under Ar atmosphere at RT for 2 hours. Disappearance of monomer peaks was monitored using ^{1}H-NMR spectroscopy. The reaction mixture was diluted with DCM and extracted with $KHSO_4$ (2x), water (1x) and brine (1x). The organic layer was collected and dried with Na_2SO_4, filtered and concentrated in vacuo. The resulting oil was precipitated in ice-cold diethyl ether and lyophilized from dioxane to yield a white powder (yield = 75-85%). ^{1}H-NMR (Figure S2): 5.17 ppm (-C=OCHCH$_3$-, 2H, multiplet), 3.63 ppm (-CH$_2$CH$_2$O-, 4H PEG, multiplet), 3.35 ppm (CH$_3$-PEG, singlet) and 1.59 ppm (C=OCHCH$_3$-, 6H, multiplet).

Synthesis of NH_2-PEG_{44}-$PDLLA_{95}$

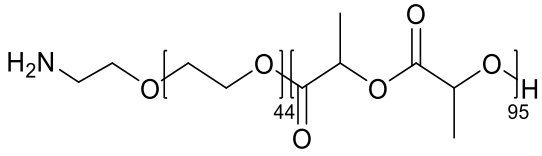

Boc-NH-PEG-OH (2 kDa, 100 mg; 0.05 mmol) was weighed into a flame-dried 50 mL round bottom flask. D,L-lactide (4.75 mmol; 0.32 gr) was added and all reagents were subsequently dried by co-evaporation with toluene. Then, dry DCM (10 mL) was added to the reaction under Argon. Afterwards, DBU (0.025 mmol; 4 µl) was added. The reaction was left stirring under Ar atmosphere at RT for 2 hours. Disappearance of monomer peaks was monitored using ^{1}H-NMR spectroscopy. The reaction mixture was diluted with DCM and extracted with $KHSO_4$ (2x), water (1x) and brine (1x). The organic layer was collected and dried with Na_2SO_4, filtered and concentrated in vacuo. The resulting oil was then dissolved using 5 mL of 4M HCl in dioxane and was stirred at RT for 2 hours to cleave the Boc-group. The solution was then concentrated in vacuo to remove HCl, dissolved in dioxane and lyophilized to yield the product as a white powder (yield = 77%). Disappearance of Boc peak (1.41 ppm, 9H, singlet) after deprotection was confirmed by ^{1}H-NMR.

Synthesis of Cy5-PEG_{44}-$PDLLA_{95}$

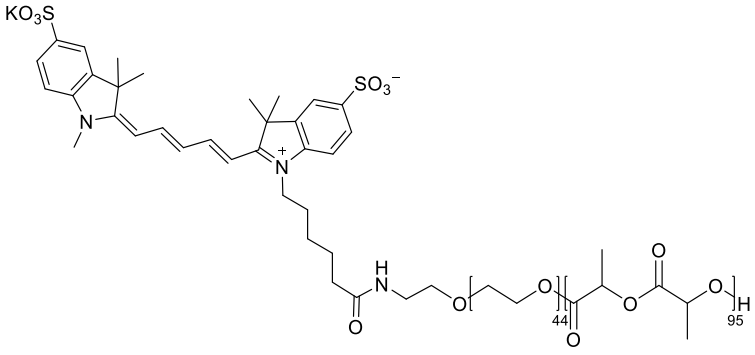

In a 10 mL round bottom flask, NH_2-PEG-PDLLA (50 mg) and sulfo-Cy5 NHS ester (1.2 eq., 2.9 mg) were dissolved in 2 mL DMF. Triethylamine (1 eq. to NH_2-R, 0.5 µL) was added after all components were dissolved. The reaction was left stirring at RT overnight. The reaction mixture was diluted with an excess of DCM and the organic layer was washed with $KHSO_4$ (1x), water (3x) (to remove dye and most of the DMF), and brine (1x). The organic layer was dried with Na_2SO_4, filtered and concentrated in vacuo. The solution was lyophilized from dioxane yielding a bright blue powder (yield = 91%).

General procedure for the preparation of stomatocytes [1]

In a 20 mL vial, PEG_{22}-$PDLLA_{95}$ and PEG_{44}-$PDLLA_{95}$ block copolymers (1:1 w/w%, 20 mg) were weighed in and dissolved in 2 mL THF/dioxane (1:4). The vial was equipped with a stirring bar (10×2 mm) and sealed with a rubber septum. A needle was inserted to release pressure. The solution was stirred at 700 rpm for 30 minutes, followed by addition of 2 mL ultrapure water with a syringe pump at a rate of 1 mL h^{-1}. The solution was then dialyzed overnight against 75 mM NaCl at 4 ℃ with a water change after 1 hour to yield stomatocytes.
For fluorescent stomatocytes (used for tumor penetration studies), Cy5-PEG_{44}-$PDLLA_{95}$ (0.5 mg; 2.5 wt%) was added to the polymer mixture before solvent displacement. The procedure is further followed as described.

General procedure for the preparation of MnO_2 nanoparticles (MnPs)

The procedure for the preparation of MnPs was adapted from literature.[3] In a 25 mL round bottom flask flushed with Argon, $KMnO_4$ (5 mM, 4 mL) was added through a septum and bubbled with Argon for 30 minutes at RT. Then, a solution of $Na_2S_2O_3$ (1.875 mM, 8 mL) was added at a rate of 1 mL min^{-1} with a syringe pump. The solution was stirred for 10 minutes, after which BSA (20 mg in 3 mL of MilliQ) was added dropwise. The solution was allowed to stir for another hour, and the solution was dialyzed against MilliQ (Spectrapor, MWCO: 1 MDa) to remove excess BSA. Samples were stored in the fridgPage e prior to use.

In situ formation of MnP-loaded stomatocytes

In a 25 mL round bottom flask flushed with Argon, $KMnO_4$ (5 – 10 mM) was dissolved in 4 mL of stomatocyte solution (5mg mL^{-1}) in MilliQ and was added through a septum. Then, the reaction mixture was bubbled with Argon for 30 minutes at RT. Thereafter, a solution of $Na_2S_2O_3$ (1.875 mM, 8 mL) was added at a rate of 1 mL min^{-1} with a syringe pump. The solution was stirred for 30 minutes, after which BSA (20 mg in 3 mL of MilliQ) was added dropwise. The solution was allowed to stir for another hour, and the solution was dialyzed against MilliQ (Spectrapor, MWCO: 1 MDa) to remove excess BSA. Samples were centrifuged down (5G, 5 mins), supernatant was removed and fresh ultrapure water was added. This was repeated until supernatant was clear. The final concentration was adjusted to obtain a polymer concentration of 5 mg mL^{-1}. Samples were stored in the fridge prior to use.

NTA motion studies

Autonomous movement of MnP-loaded stomatocytes was carried using nanoparticle tracking analysis technique. To do so, stomatocytes were suspended in PBS solution (1x) to yield an approximate concentration of 10 µg mL^{-1} (between 10^7 and 10^9 particles mL^{-1}). For a typical experiment, 1 mL of sample (ca. 10 µg mL^{-1}) was loaded in the NTA chamber using a syringe. Thereafter, the particles' movement was recorded for 30 seconds. The same measurement was performed for 4 times so that reproducibility can be ensured. The NTA software was used to track the nanomotors. In order to study the active motion of the MnP-loaded stomatocytes, an aliquot of hydrogen peroxide, as a fuel, was added to the diluted sample and the measurements were started immediately after mixing.

Multiple fuel addition cycles were performed to demonstrate the system's stability (Figure 2D, main manuscript). To do this, MnP-loaded stomatocytes were diluted (1:1000) in 1x PBS and subsequently injected into the NTA chamber. Brownian motion of hybrid nanomotors was monitored in the absence of fuel. Thereafter, sample was extracted from the NTA chamber, an aliquot of H_2O_2 was added (to reach the desired H_2O_2 concentration), and motility was immediately recorded. To ensure complete fuel depletion, the nanomotors were left at RT for 24 hours. The same experiment was repeated twice using the same nanomotor sample.

Movement analysis

NTA was used to study the autonomous motion of stomatocytes in absence and presence of fuel and calculate their mean squared displacement (MSD), following previously published procedures. The motion of the stomatocytes in presence of fuel, at different concentrations of H_2O_2, was measured by tracking both the X and Y coordinates of at least 25 particles for 30 seconds. MSD curves were extracted from NTA recorded trajectories using the equation $MSD = \langle \Delta r^2(t) \rangle = \langle \frac{1}{N} \sum_{i=0}^{N} (r_i(t) - r_i(0))^2 \rangle$ where r = radius and t = sampling time and MSD(t) = 2dD, where D = diffusion coefficient and d = dimensionality (NTA measurements have dimension d = 2).
The equation MSD = $(4D)\Delta t + (v^2)(\Delta t^2)$ was used to fit the MSD curves. From the fitting of the MSD curves, the average particle velocity can be extracted. According to the particle diffusion coefficient, as described by Galestonian's diffusiophoretic model, a particle undergoing Brownian motion will display a linear MSD over time with the slope determined by the diffusion coefficient $D = K_B T/(6\pi\eta R)$. From this model, if the particles are in Brownian motion, the linear component of the MSD, according to the equation MSD = $(4D)\Delta t$, can be extracted. Indeed, in the absence of fuel, a linear relation between MSD and time was observed. The same linear relationship

was also observed when empty stomatocytes were exposed to fuel, highlighting the significance of catalytic species in driving the motors' thrust (figure S11A). On the contrary, addition of fuel to the MnP-loaded nanomotors resulted in observable autonomous motion (video S2). Although our hybrid nanomotors (average radius = 200nm) display fast rapid self-rotation (ca. 0.05s), with rotational diffusion described by $D_r = \tau_r^{-1} = TK_B/(8\pi\eta R^3)$ (where τr is reorientation time), the MSD curves (at high fuel concentration and $\Delta t > \tau r$) displayed a parabolic fit. This was also observed in previously published stomatocyte nanomotors. It is therefore our hypothesis that the reason behind this behavior could be a result of the unique stomatosomal morphology, also in combination with the bubble-generation mechanism that counteract the effects of rapid τr. These suggested mechanisms are hypotheses and theoretical and experimental confirmation are on-going research in our group.

Cell viability of MnP-loaded stomatocytes

HeLa cells were cultured in DMEM medium containing 10 % FBS, 1 % penicillin/streptomycin (complete DMEM) in 5 % CO_2 at 37 °C. The cell viability in presence of stomatocytes was evaluated in vitro using an MTT assay. The cells were seeded in 96-well plates at a density of 5×10^3 cells per well in 100 µL DMEM medium and were cultured for 24 h at 37 °C. Subsequently, the cells were incubated with empty stomatocytes (containing 1% Cy5-PEG-PDLLA) and MnP-loaded stomatocytes (containing 1% Cy5-PEG-PDLLA) for 24 h, respectively. The cells were washed and fresh medium containing MTT was added into each well. The cells were incubated for another 4 h. After removing the medium containing MTT, dimethyl sulfoxide (100 µL) was added to each well to dissolve the formazan crystals. Finally, the plate was gently shaken for 5 min and the absorbance at 490 nm was recorded with a micro-plate reader.

Cell rescue studies

HeLa cells were cultured in DMEM medium containing 10 % FBS, 1 % penicillin/streptomycin in 5 % CO_2 at 37 °C. The cell viability in presence of H_2O_2 was evaluated in vitro by an MTT assay. The cells were seeded in 96-well plates at a density of 5×10^3 cells per well in 100 µL DMEM medium and cultured for 24 h at 37 °C. Subsequently, the cells were incubated with 125 or 250 µM H_2O_2 and either 125 µg/mL or 250 µg/mL MnP-loaded stomatocytes for 24 h. The cells were washed and fresh medium containing MTT was added into each plate. The cells were incubated for another 4 h. After removing the medium containing MTT, dimethyl sulfoxide (100 µL) was added to each well to dissolve the formazan crystals. Finally, the plate was gently shaken for 5 min and the absorbance at 490 nm was recorded with a micro-plate reader.

S3. Supplementary Figures and Tables

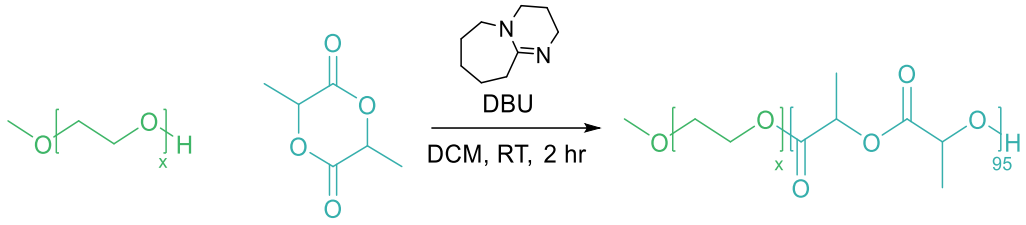

Figure S1. Ring opening polymerization of D,L-lactide and mPEG into PEGx-PDLLA95, with x=22/44

Table S1. Analysis of PEG_x-$PDLLA_{95}$ block copolymers for preparation of stomatocytes

Polymer	Composition by ^{1}H-NMR	Đ from GPC
PEG_{22}-$PDLLA_{95}$	PEG_{22}-$PDLLA_{98}$	1.17
PEG_{44}-$PDLLA_{95}$	PEG_{44}-$PDLLA_{95}$	1.11
H_2N-PEG22-$PDLLA_{95}$	H_2N-PEG_{44}-$PDLLA_{89}$	1.09
Cy5-PEG22-$PDLLA_{95}$	Cy5-PEG_{44}-$PDLLA_{89}$	1.21

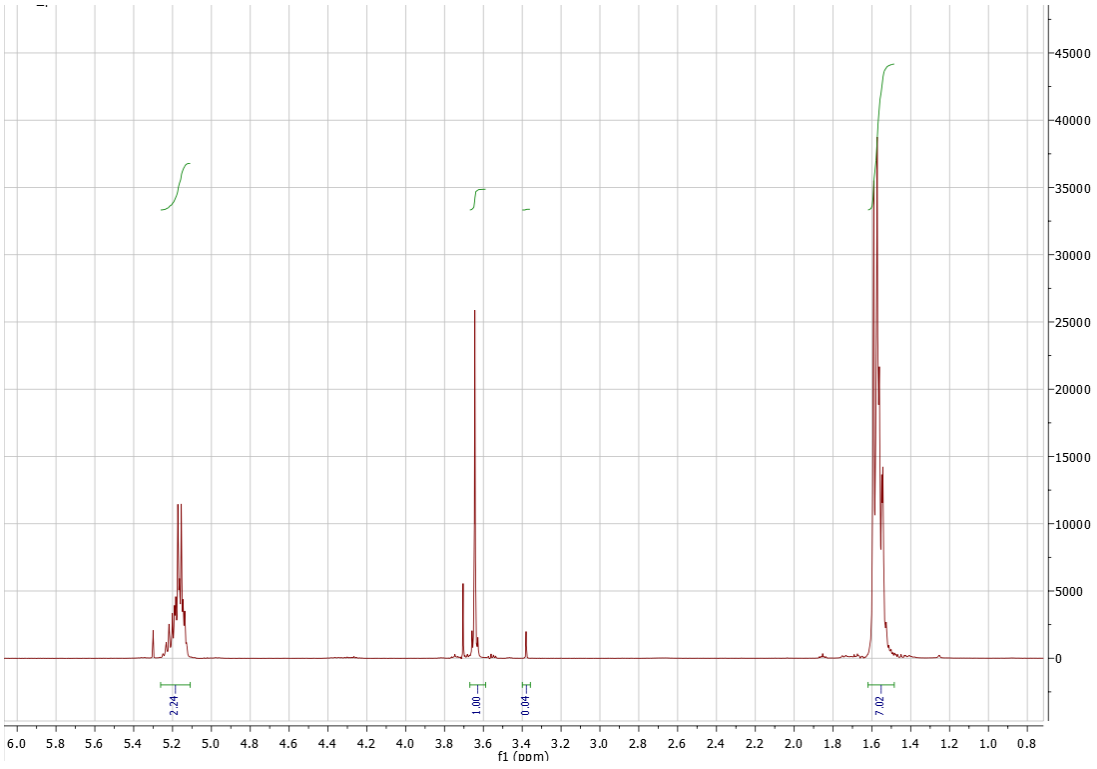

Figure S2. Typical ^{1}H-NMR spectrum of PEG_{22}-$PDLLA_{95}$ polymer.

Analysis of stomatocytes

To verify the structure of stomatocytes, Dynamic Light Scattering (DLS), Nanotracking Analysis (NTA) and cryo-Transmission Electron Microscopy (cryo-TEM) studies were performed. For DLS, samples were prepared by diluting the stomatocyte solution (10x) in ultrapure water and the measurement was performed in a disposable cuvette. Size data was extracted from Intensity plots. NTA studies were performed by diluting the stomatocytes (1000x) in ultrapure water so that a minimum of 20 particles were visible within the measuring frame. Samples were recorded for 30 seconds and a minimum of 5 runs. For cryo-TEM analysis, the sample was used undiluted. Images were analyzed using ImageJ software.

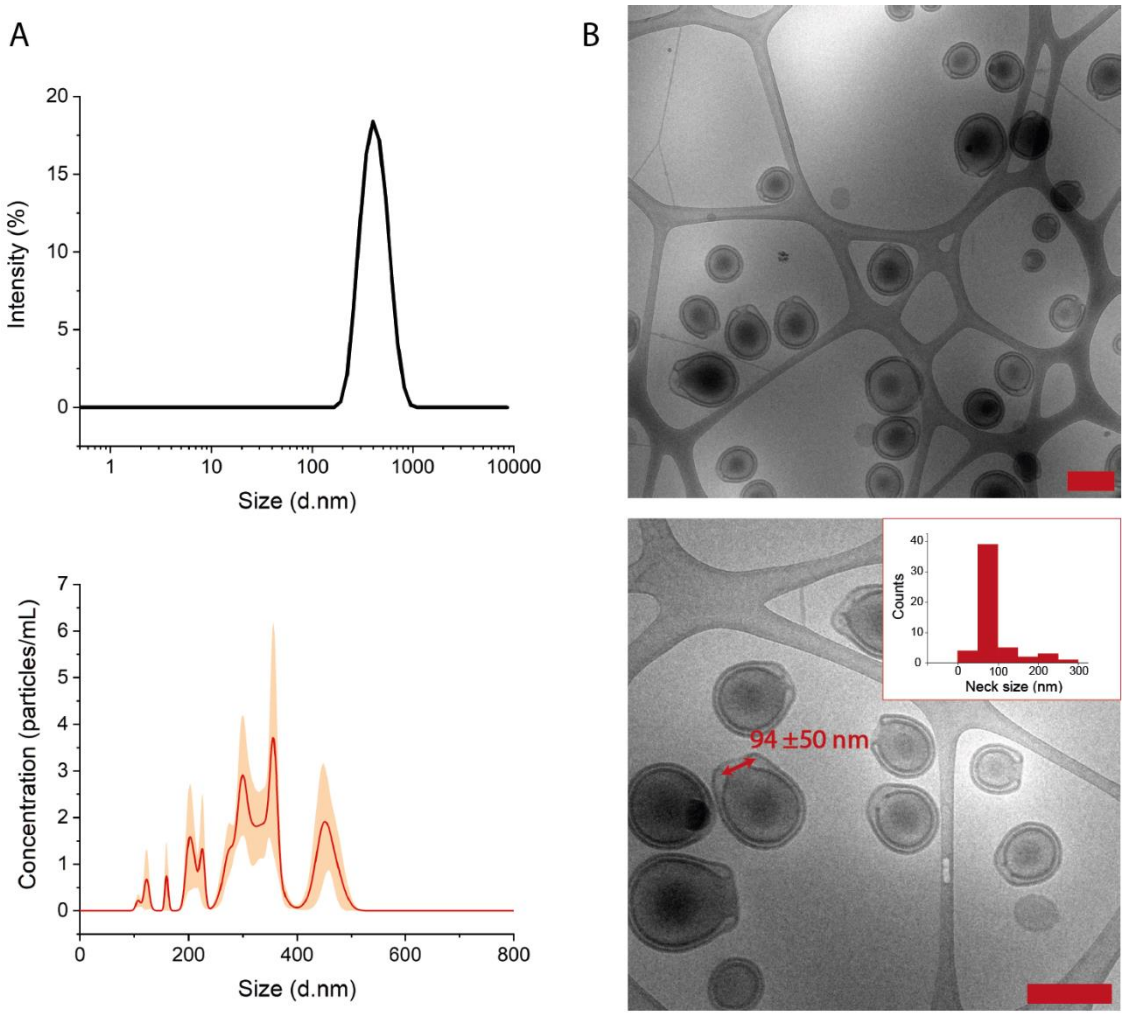

Figure S3. A) Dynamic light scattering (DLS) intensity plot and nanotracking analysis (NTA) and B) Cryo-TEM images of $PEG_{22/44}$-$PDLLA_{95}$ stomatocytes. Insert displays neck size distribution of 50 stomatocytes. Scale bars = 500 nm.

Tomography of MnP-loaded stomatocytes

To visualize the spatial distribution of MnPs inside the stomatocyte lumen, (cryo-)TEM tomography experiments were performed. Sample preparation was performed as described in section S1 (Experimental Materials and Methods). Suitable MnP stomatocytes were tracked in the sample in which reference particles were abundant. In a typical experiment, 3 µL of suspended 20 nm fiducial gold nanoparticles were added to 27 µL of sample and mixed gently. Tilt-series acquisition was performed over an angular range of ±66 degrees with 3 degrees increments, at a nominal magnification of 11.5 kx and a nominal defocus of -7.5 µm. The gold markers were used for alignment of the tilt series with respect to a common origin and tilt axis and reconstructed using IMOD software.[4] The 3D reconstruction was manually segmented into stomatocyte's (green) and MnO_2 (gray) and visualized by surface rendering and volume texture using Avizo software (Thermo Fisher Scientific).

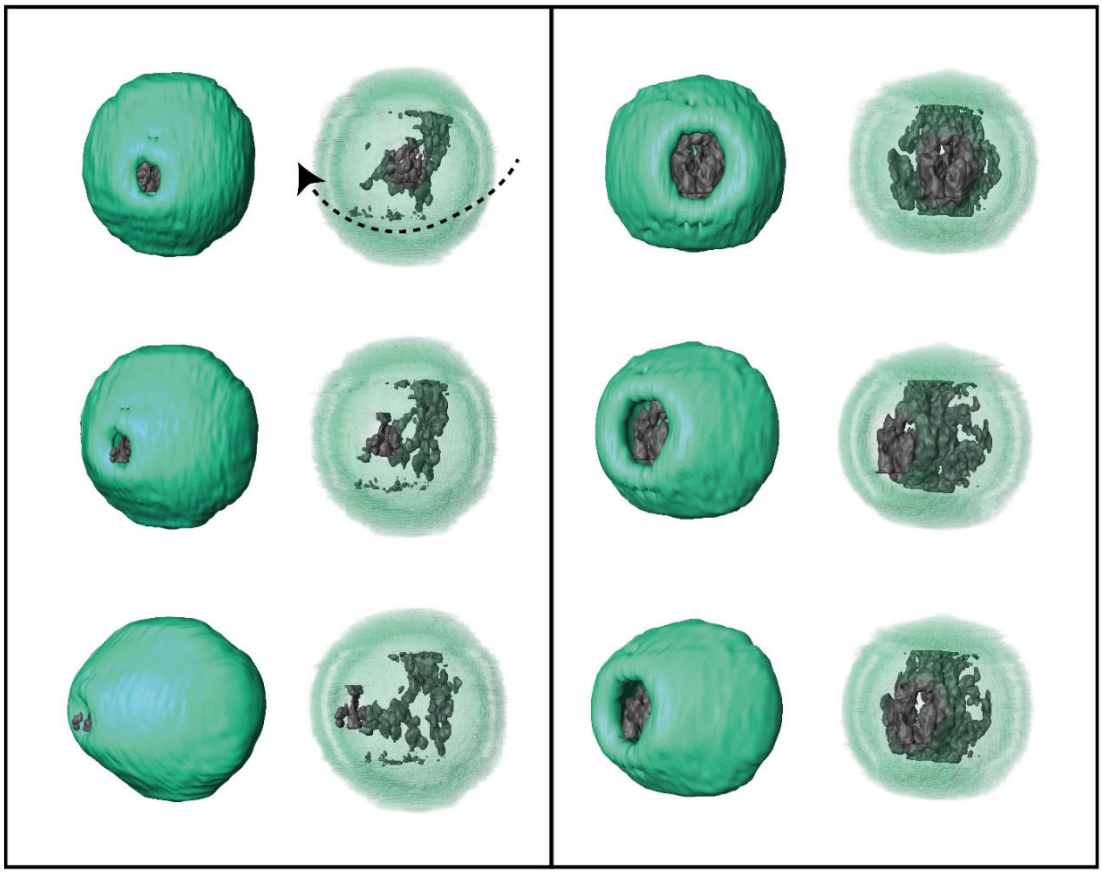

Figure S4. Segmentation results of cryo electron tomography showing stomatocyte (green) and MnO_2 (gray) using isosurface (left column) and volume texture (right column) rendering.

The sequence of the formation of the hybrid nanomotor is: (i) addition of $KMnO_4$ to a stomatocyte solution results in the distribution of MnO_4^- ions in the solution and in the cavity, (ii) addition of dithionate (reducing agent/nucleation trigger) triggers the reduction of Mn(VII) to form MnO_2 crystals which nucleate into nanoparticles, (iii) as nanoparticle formation is kinetically more favorable than their diffusion out of the cavity several nanocrystals coexist within the cavity, (iv) any leakage during the formation process is counteracted by diffusion of nanoparticles from the rich environment, (v) nanoparticles in close proximity within the cavity aggregate into bigger assemblies as (evidenced from microscopy images), (vi) as nanoparticle clusters have a larger size than the stomatocyte neck, they remain trapped during the washing steps, finally yielding the nanomotor structure.

Cryo-TEM analysis of MNP stomatocytes

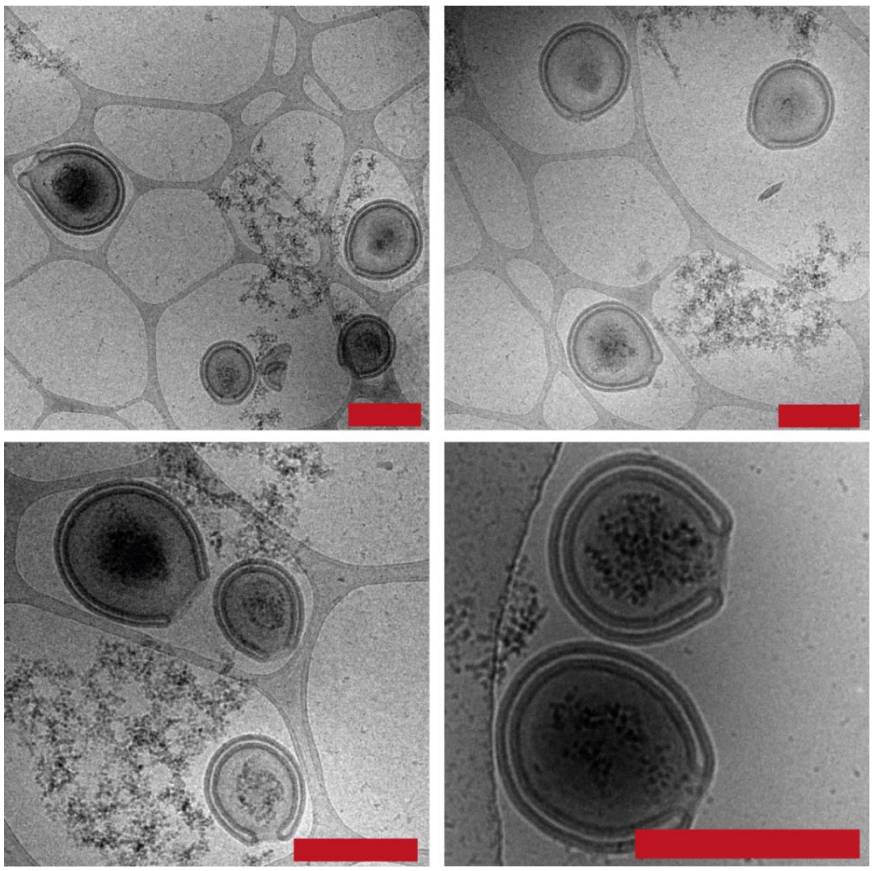

Figure S5. Cryo-TEM images of MnP-loaded stomatocytes (unpurified). Scale bar = 500 nm.

Purification of MnP-loaded stomatocytes

To separate free MnPs from MnP-loaded stomatocytes, centrifugation was performed. Samples containing 500 µL MnP-loaded stomatocytes were spun in a 1.5 mL Eppendorf® at 5g for 5 minutes. The supernatant containing free MnPs was removed and new medium was added. Thereafter, samples were re-dispersed by vortexing. This was repeated until the supernatant no longer contained free particles, after which new medium was added and particles were resuspended with vortexing and sonication.

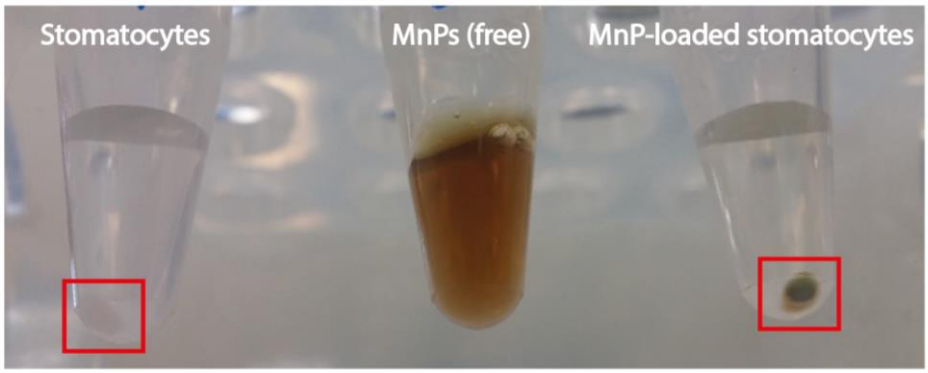

Figure S6. Visual showing the result of centrifugation to remove free MnPs. The samples are shown after centrifugation with pellets (of stomatocytes) visible on the left and right whilst free MnPs remain in supernatant due to their small size. On the right, the supernatant is clear of free MNP after several centrifugation cycle

Attempts to encapsulate preformed inorganic nanoparticles (including MnO_2) within the cavity of PDLLA stomatocytes

Preceding development of the herein reported compartmentalized synthesis approach, physical encapsulation of preformed nanoparticles was assessed. One such method involved statistical engulfment of nanoparticles in the stomatocytes' cavity during formation - following previously methods applied to polystyrene-based polymersomes.[5] Typically, nanoparticles were added prior to the shape transformation process. Attempts to carry out similar encapsulation processes using PDLLA polymersomes and a variety of inorganic nanoparticles were not successful. Analysis of cryo-TEM images showed no encapsulation, and in most of the cases unsuccessful formation of stomatocytes

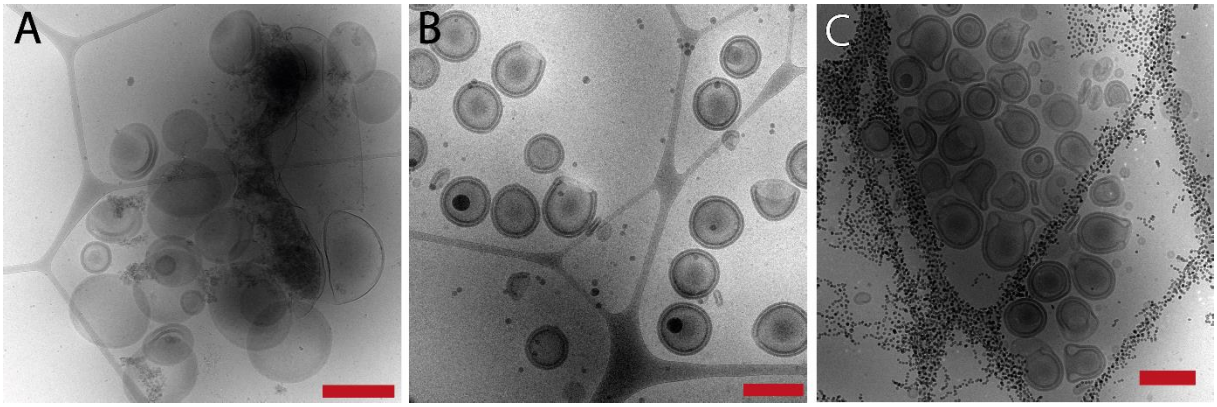

Figure S7. Cryo-TEM images of the results from encapsulation of preformed inorganic nanoparticles inside PDLLA-based stomatocytes. A, B) attempts to encapsulate MnO_2 nanoparticles. Both stomatocytes and polymersomes were formed - no encapsulation was observed. C) Attempts to encapsulate Fe_3O_4 (magnetite) nanoparticles. Scale bars = 500 nm

Analysis of free MnPs in solution

First, non-encapsulated MnPs were separated from the nanomotors by centrifugation. Free MnPs were then diluted 10-fold in ultrapure water and measured in a disposable cuvette.

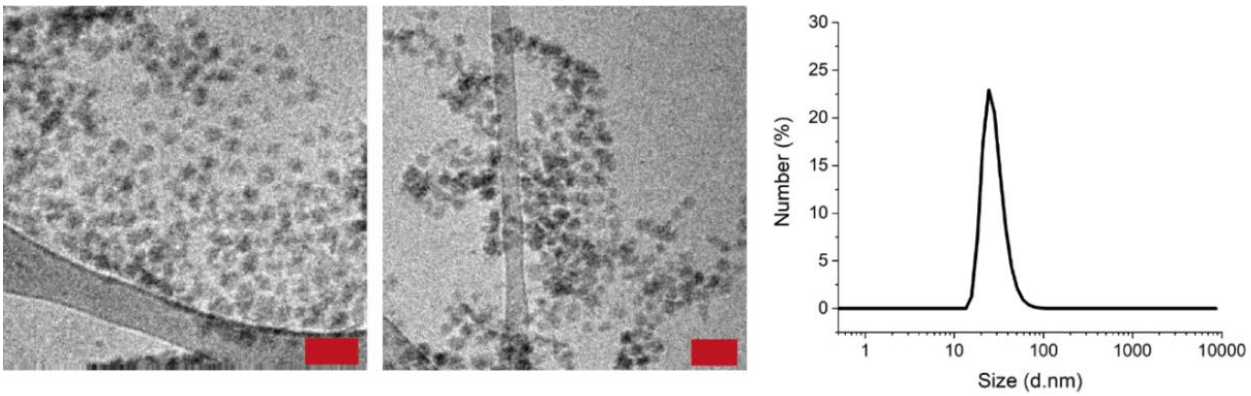

Figure S8. DLS and cryo-TEM measurements of MnO_2 nanoparticles (MnPs) free in solution. Scale bars are 100 nm.

MSD curves of MnP-loaded stomatocytes in the absence and presence of fuel at varying concentrations

As displayed in Figure 2 in the main manuscript, the presence of fuel affects the Brownian motion of MnP-loaded stomatocytes and induced autonomous motion. To this end, NTA measurements were performed by diluting MnP-loaded stomatocytes ([polymer] = 5 mg mL^{-1}) 1000-fold in 1x PBS. Thereafter, aliquots of H_2O_2 were added (to reach a final concentration of 5, 25 and 50 mM). The dotted line is the average of all MSD curves calculated and the colored areas depict the standard deviation of these curves.

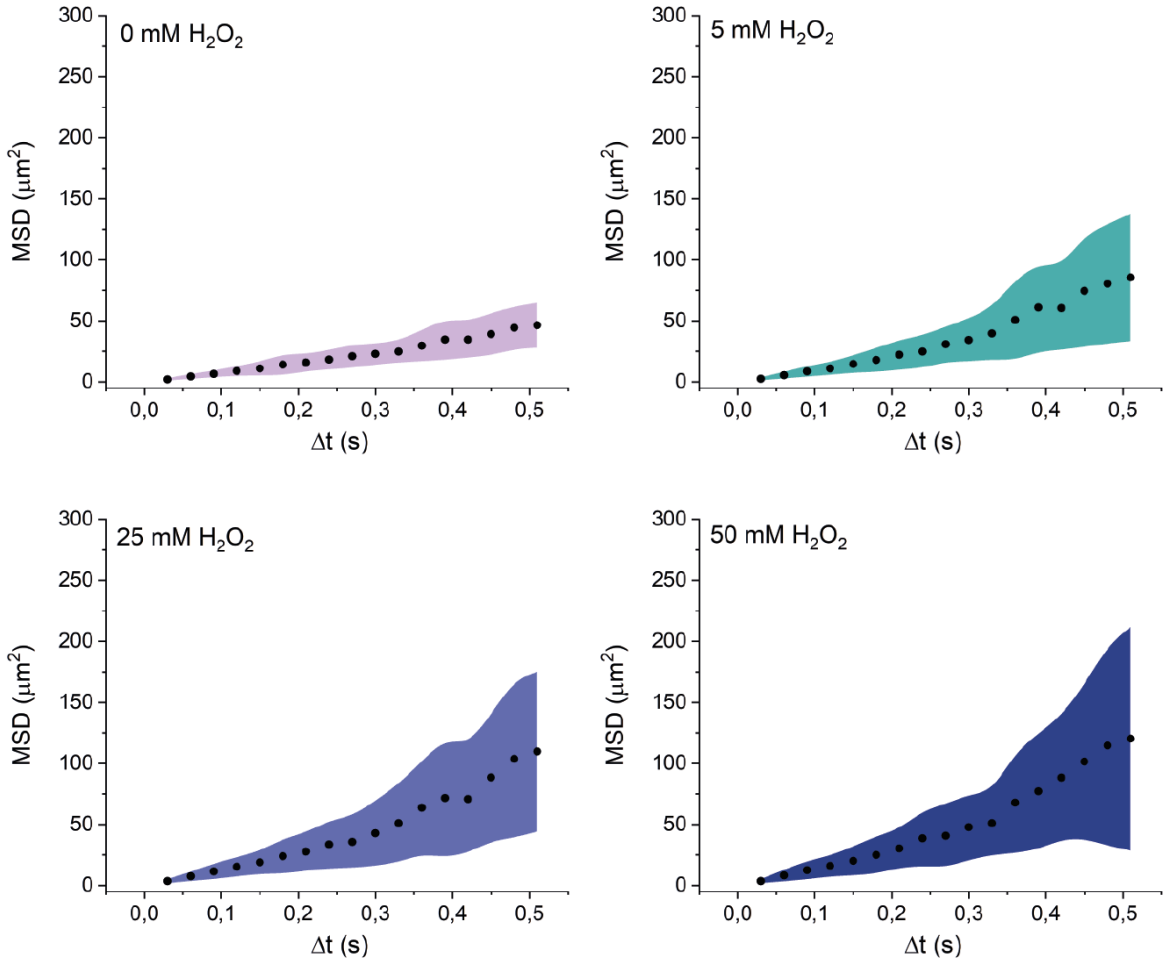

Figure S9. Average MSD curves and standard deviation (colored) of MnP-loaded stomatocytes in presence of fuel at varying concentrations.

Anomalous Diffusion Exponent (α)

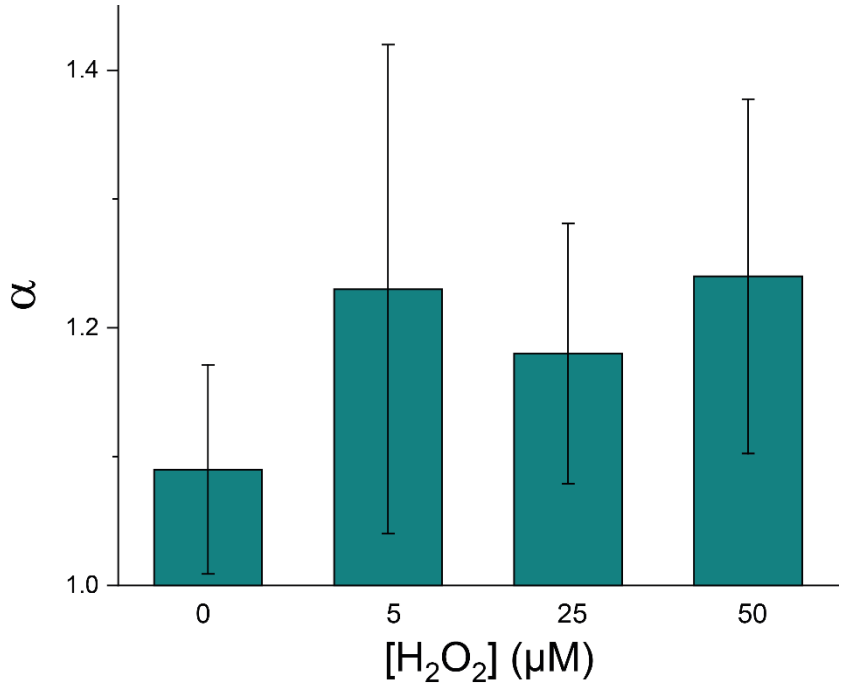

Figure S10. Analysis of the anomalous diffusive exponent (α value). Please note the increase of α value after addition of fuel – this suggests enhanced super-diffusion (propulsive) behavior.

Diffusion coefficients of unloaded stomatocytes with or without free MnPs

To determine whether the Brownian motion of empty stomatocytes was affected by the presence of fuel, NTA motion analysis was performed on empty stomatocytes (1000-fold dilution of stomatocytes (5 mg mL^{-1}) in 1x PBS), to which fuel was added (to reach a final concentration of $[H_2O_2]$=100 mM). The diffusion coefficients were extracted from the data and are plotted below. Additionally, to demonstrate that the design of hybrid stomatocytes is necessary for enhanced motion, 1 µL of as-prepared MnPs (1.4 mM solution) were combined with 1 µL of empty stomatocytes (5 mg mL^{-1}) and diluted with 998 µL PBS (1x). An aliquot of fuel (so that final concentration $[H_2O_2]$ = 100 mM) was added and samples were measured immediately. Indeed, no increase in diffusion coefficients in the presence of fuel was observed, indicating that propulsion of stomatocytes did not take place.

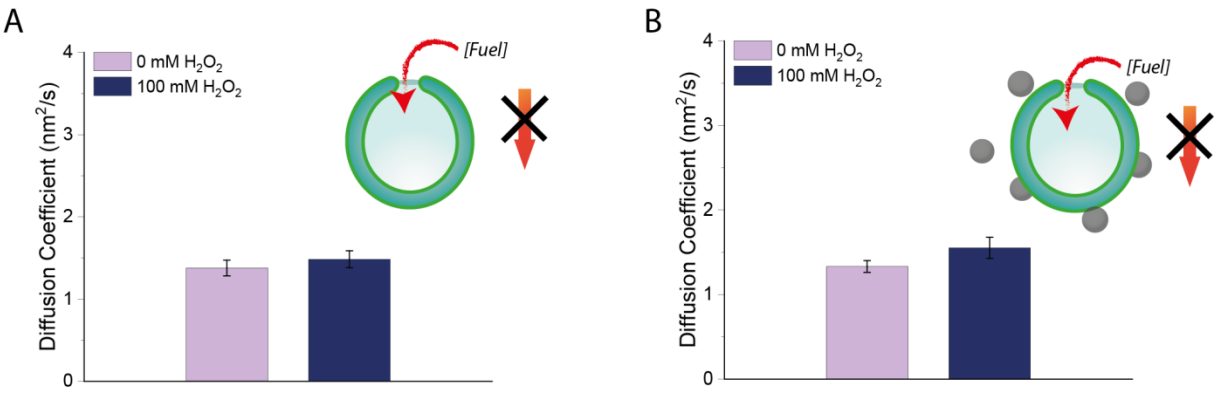

Figure S11. Diffusion coefficients of unloaded stomatocytes (A) and unloaded stomatocytes with free MnPs (B) in the absence and presence of fuel. There is no increase in diffusion, indicating that the design of the hybrid stomatocyte is imperative to its functionality.

Stability of stomatocytes and catalyst in the presence of proteinase K

To verify the physical stability of both MnPs and hybrid stomatocytes, proteinase K (in PBS, to reach a final concentration of 50 µg mL^{-1}) was added to a 10-fold diluted sample (in 1x PBS). The solution was left standing for 30 minutes at RT before measuring DLS. Indeed, size and dispersion of the MnPs remained the same in the presence of proteinase K. However, for hybrid stomatocytes, a slight increase in particle size is observed. This result is in correspondence with Figure 2E in the main manuscript, where particles' Brownian motion seemed to be affected by the presence of proteinase K, a direct result of particle size.

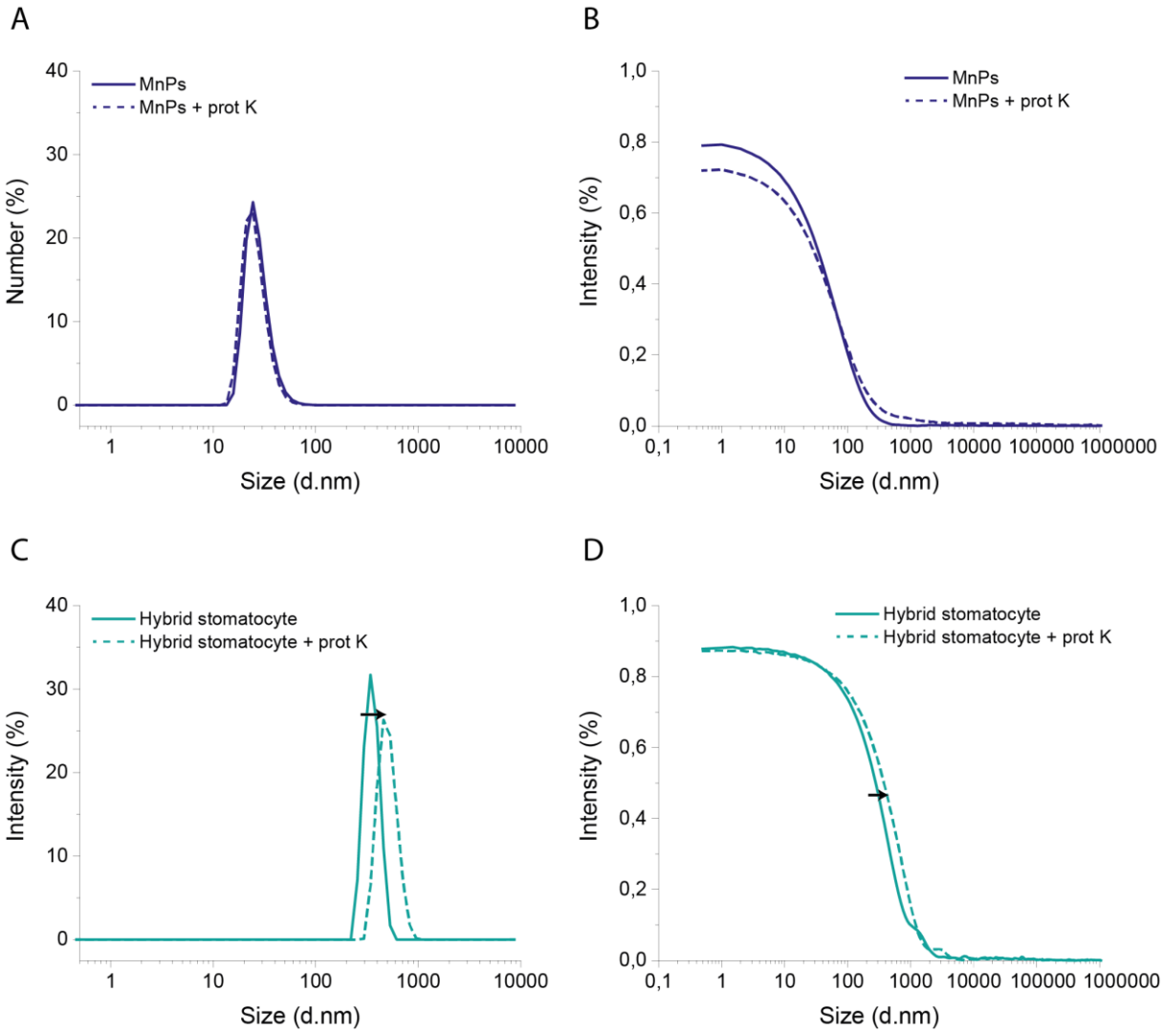

Figure S12. DLS size distribution plots and correlograms of samples in PBS, with or without proteinase K. A) Number plot and B) correlogram of MnPs in PBS. C) Intensity plot and D) correlogram of hybrid stomatocytes in PBS. For the stomatocytes, the presence of proteinase K causes a slight increase in size, most likely due to protein interactions on the surface of the stomatocyte.

MSD of empty stomatocytes in the presence of proteinase K

In Figure 2D, the MSD of MnP-loaded stomatocytes in the presence of proteinase K is decreased in the absence and presence of fuel, most-likely due to protein absorption on the surface of the stomatocytes. This was also verified in Figure S12, where a size increase is clearly visible from DLS measurements of MnP-loaded stomatocytes with proteinase K. This phenomenon was further investigated using empty stomatocytes. To this end, 1 µL of stomatocyte solution ([polymer] = 5 mg mL^{-1}) was diluted 1000-fold in 1x PBS and proteinase K solution (to reach a final concentration of [ProK] = 50 µg mL^{-1}, in 1x PBS) was added. The solution was left at RT for 1 hour before measuring using NTA.

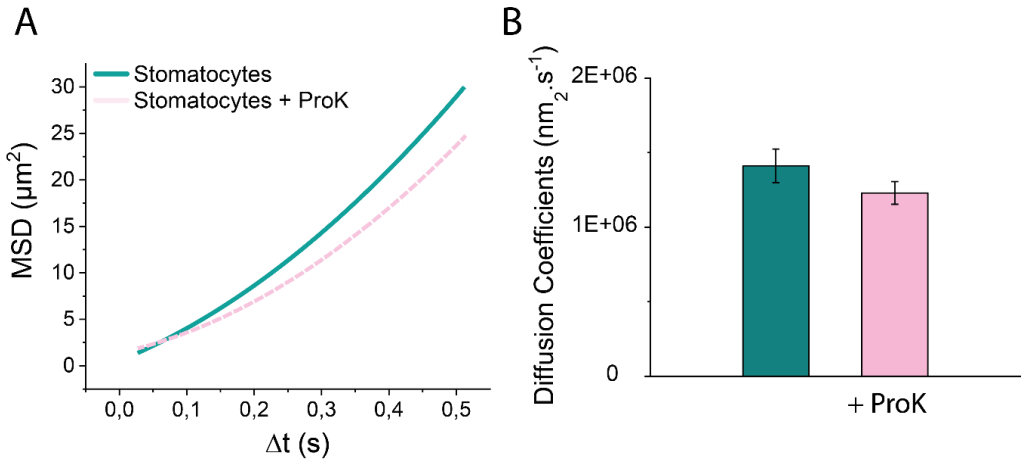

Figure S13. MSD (A) and diffusion coefficients (B) of stomatocytes in PBS with or without addition of proteinase K. Indeed, a slight decrease is visible in both MSD and diffusion coefficient, indicating that proteinase K affects the Brownian diffusion of stomatocytes.

Batch-to-Batch size variation of MnP-loaded stomatocytes

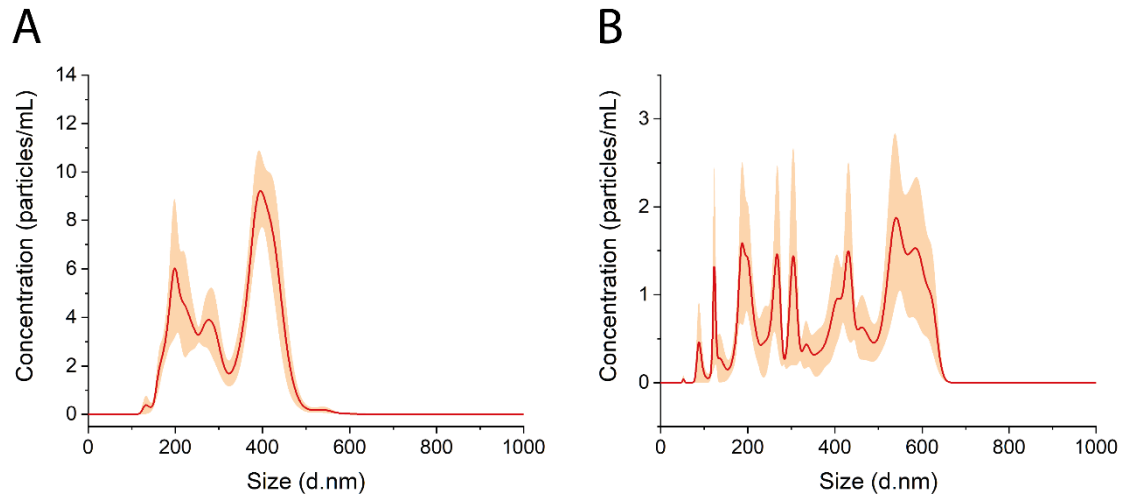

Figure S14. Size distributions as measured with NTA for samples used in the main text (A) in Figure 2 and (B) in Figure 3. Please note: such batch-to-batch variation is normal and widely observed within polymeric self-assembled systems.

Activity of MnP-loaded stomatocytes in low concentrations of GSH

To determine whether the stomatocytes would remain active and stable in physiological conditions, MnP-loaded stomatocytes were exposed to low concentrations of GSH (10 µM).

The stability of free MnPs was determined by diluting 100 µL as-prepared MnP solution in 900 µL 10x PBS. The solution was stirred and an aliquot of GSH (so that final concentration [GSH] = 10 µM, in 10x PBS) was added to the solution while stirring. The particles were recorded for 1 minute (**Figure S15A**)

To investigate the enhanced diffusion of MnP-loaded stomatocytes in these conditions, 1 µL stomatocytes ([polymer] = 5 mg mL^{-1}) were diluted 1000-fold 10x PBS and an aliquot of GSH was added (so that final concentration [GSH = 10µM). Then, an aliquot of H_2O_2 was added ([H_2O_2 (final)] = 100 mM) and NTA measurement was carried out immediately. Clear autonomous motion can clearly be observed in presence of fuel.

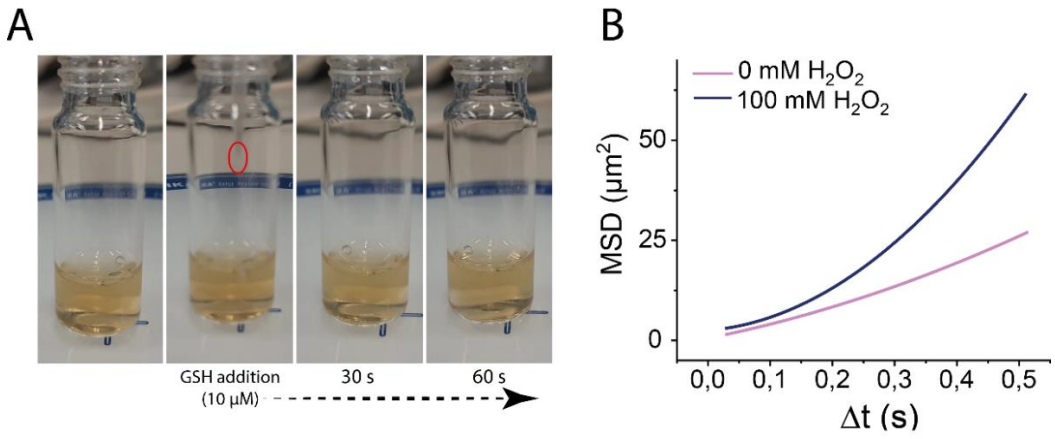

Figure S15. Images depicting stability of free MnPs in the presence of 10 µM GSH in PBS (A) and activity of MnP-loaded stomatocytes in the presence of 10 µM GSH and fuel (B) in PBS. Particles do not degrade within the measured time-frame and still demonstrate activity, whereas the nanomotors in the presence of endolysosomal concentrations GSH were immediately deactivated.

Table S2. Table depicting all numerical values for cell viability assay depicted in figure 4A.

	15.62	31.25	62.5	125	250	[Concentration stomatocytes µg mL^{-1}]
Empty Stomatocytes	99 ± 10	96 ± 8	93 ± 11	89 ± 9	82 ± 7	[Cell viability %]
MnP-loaded stomatocytes	103 ± 10	94 ± 10	91 ± 11	87 ± 8	84 ± 9	[Cell viability %]

Cell rescue studies – negative control

Procedure as described in section S2. Cell viability was tested in the presence of 125 and 250 μM H_2O_2 where no viable cells were detected. No increase in viability was observed after addition of 125 or 250 μg mL^{-1} of unloaded stomatocytes; validating the importance of an active component inside the stomatocyte cavity to rescue cell viability (Figure 4B of the main manuscript).

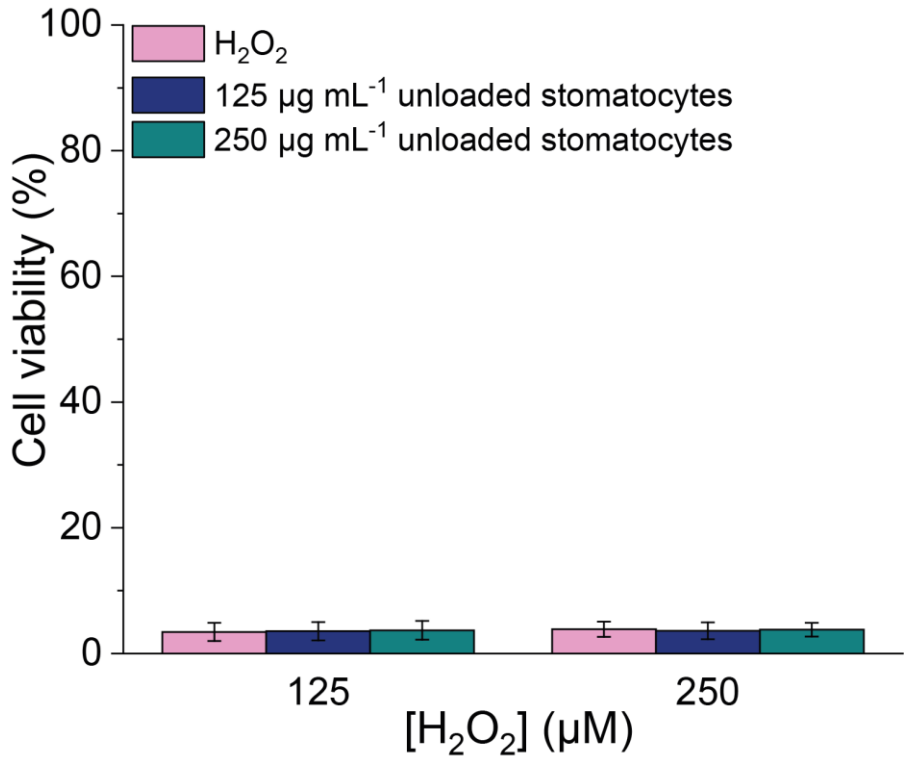

Figure S16. Cell viability assay of HeLa cells in the presence of 125 and 250 μM H_2O_2 and the same concentrations of unloaded stomatocytes.

Enhanced diffusion of MnP-loaded stomatocytes in low concentrations of H_2O_2

To verify the nanomotor's activity in low concentrations of H_2O_2, NTA measurements of MnP-loaded stomatocytes were carried out by diluted MnP-loaded stomatocytes ([polymer] = 5 mg mL^{-1}) 1000-fold in 1x PBS. Then, aliquots of H_2O_2 (to reach final concentrations [H_2O_2] = 125 µM or 250 µM, corresponding to the fuel concentrations used in cell assays described in this paper) were added and samples were measured using NTA. MSD, diffusion coefficients and trajectories were extracted from NTA data.

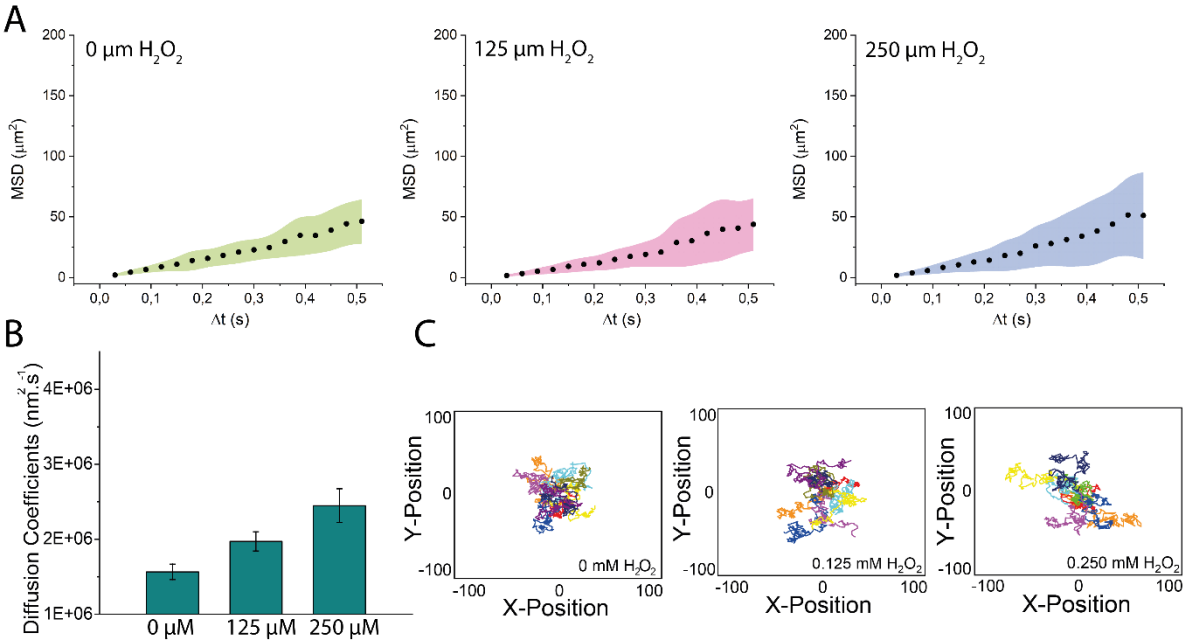

Figure S17. (A) MSDs of MnP-loaded stomatocytes in the absence and presence of 125 and 250 µM H_2O_2, their corresponding diffusion coefficients with standard error (B) and trajectories (C). The stomatocytes demonstrate nanomotor behavior in low fuel concentrations.

Table S3. Table depicting all numerical values for cell viability assay of nanomotors in the presence of fuel (Figure 4B)

	125 µM H_2O_2	250 µM H_2O_2	
PBS	3.9 ± 1.3	3.4 ± 1.4	[Cell viability %]
125 µg mL^{-1} nanomotors	53.6 ± 8.7	13.5 ± 1.8	[Cell viability %]
250 µg mL^{-1} nanomotors	78.9 ± 5.8	44.6 ± 3.8	[Cell viability %]

Presence of ROS in HeLa cells

The ROS shielding effect of MnP-loaded stomatocytes was studied using confocal microscopy imaging. HeLa cells were cultured in DMEM medium containing 10% FBS, 1% penicillin/streptomycin in 5% CO_2 at 37 ℃. HeLa cells were seeded in an 8 well µ-slide for 24 hours after which medium was refreshed. The cells were treated simultaneously with 250 µM H_2O_2 and 250 µg mL^{-1} MnP-loaded stomatocytes and were left incubating for 24 hours. Then, the cells were washed and subsequently loaded with CM-H2DCF. Thereafter, the cells were stained with Hoechst 33342 for 10 minutes. The cells were washed with PBS buffer (pH 7.4) three times. Fluorescent images were captured using a Leica TCS 264 SP5X microscope system. Overlays were prepared in ImageJ.

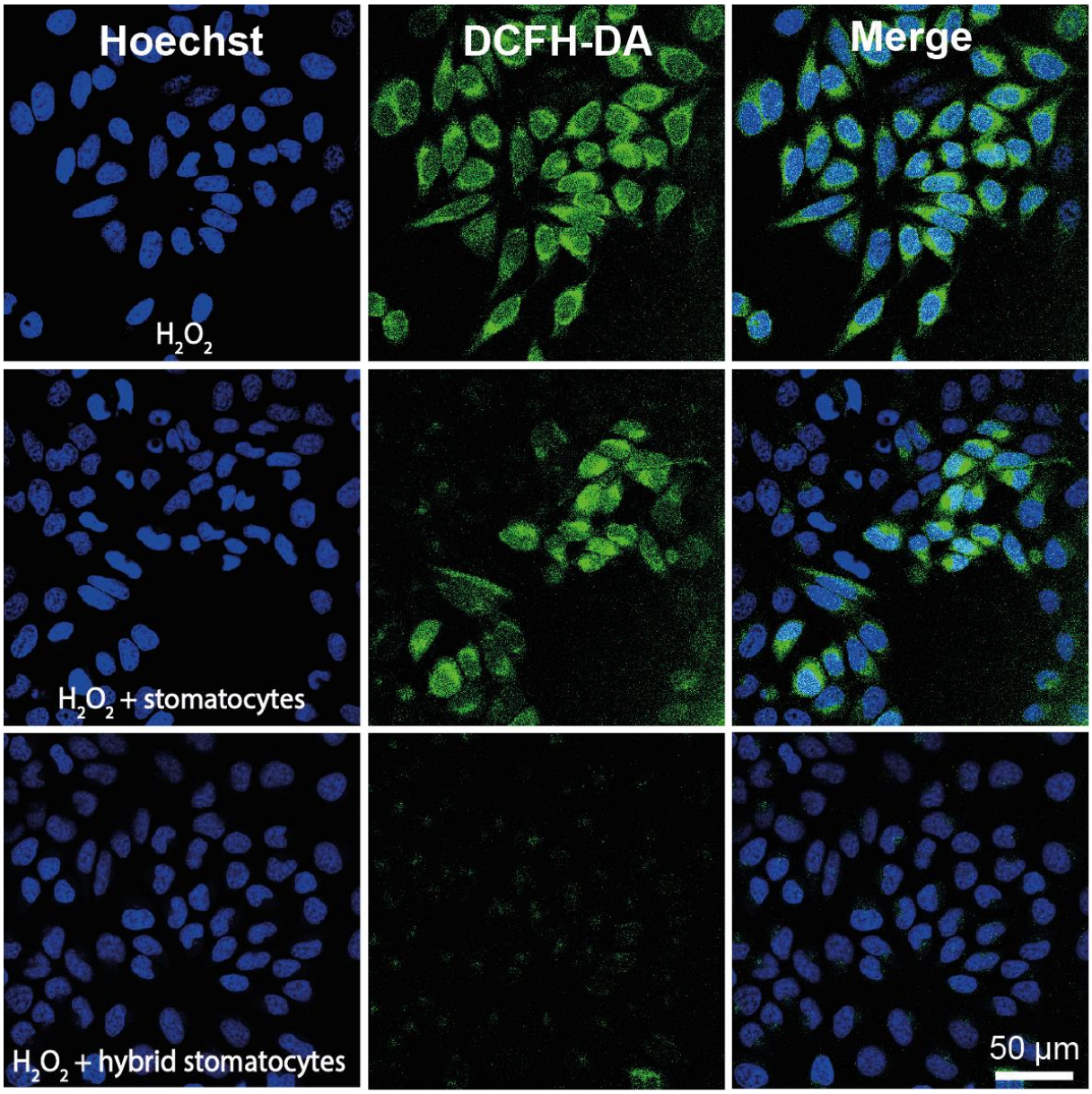

Figure S18. Confocal fluorescent images of HeLa cells incubated with H_2O_2, either in the absence or presence of empty stomatocytes or hybrid stomatocytes. Hoechst shows cell nucleus, DFCH-DA shows ROS levels and the overlay shows the presence of ROS for all cells in image.

Corrected total cell fluorescence (CTCF)

To quantify whether cells indeed show decreased fluorescent signal (indicating decrease in ROS), the corrected total cell fluorescence (CTCF) can be calculated. A total fluorescent signal irrelevant of cell area does not quantify the fluorescence of an imaged cell. Instead, the CTCF considers the cell area for each measured cell. The formula CTCF= Integrated Density – (Area of Selected Cell * Mean Fluorescence of Background) is used to accurately determine the fluorescent signal of CM-H2DCFDA in 15 HeLa cells from confocal images using imageJ to measure the intensity values. From these values, the effect of hybrid stomatocytes on the ROS levels in HeLa cells can be seen from a decreased CTCF signal, in correspondence with the confocal images from figure S18, indicating that the hybrid stomatocytes are indeed active in biological medium and can effectively consume H_2O_2.

This ROS shielding effect correlated to an increase of cell viability up to 45 % (Figure 4B, main manuscript). Fluorescence reduction of the ROS indicator CM-H2DCF is not an exact monitor of viability (as compared to the MTT assay) and even major reduction in this signal (as shown in Figures S18 and below) is not commensurate with total cell survival. This effect in cell viability could be attributed to a certain extent of cell damage during incubation with H_2O_2 and the nanomotor, prior to H_2O_2 consumption.

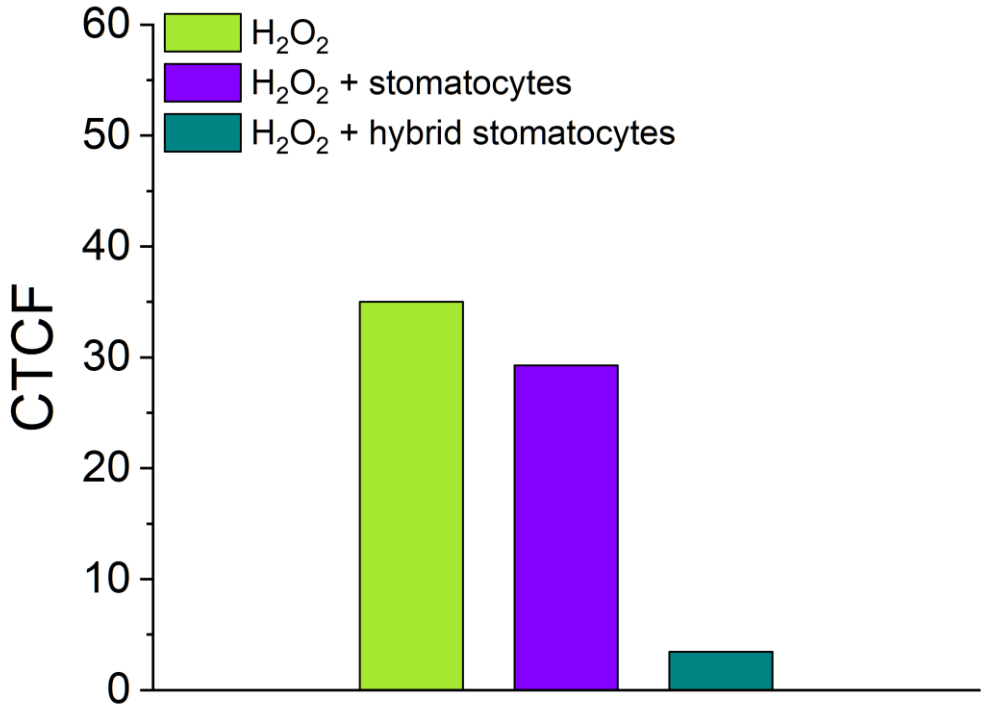

Figure S19. Corrected total cell fluorescence of the confocal images depicted in figure S18

Penetration studies with 3D multicellular spheroids (MCSs)

3D multi-cellular spheroids (MCSs) were prepared according to a literature procedure with slight modifications.[6,7] Agarose coated 96-well plates were prepared first. In detail, 0.15 g of agarose was added to 10 ml of low glucose DMEM (1.5% wt/vol) in an appropriate beaker, sealed with aluminum foil or a lid and autoclaved for 20 min at 120 ℃. Next, 50 µl of the hot (80~90 ℃) solution was added to each well of a 96-well plate (flat bottomed) under sterile conditions. The agarose solidified within seconds to minutes to produce a concave surface. HeLa cells (200 µL, 1 × 104 cells mL^{-1} in high glucose DMEM medium) were cultured in the above agarose-coated 96-wel plates, followed by incubation at 37 °C with 5% CO_2 humidified atmosphere for 4 days for the production of MCSs. Then the spheroids were incubated with 250 µM H_2O_2 and 250 µg/mL Cy5 labeled MnP-loaded stomatocytes for 4 h, the Cy5 labeled blank stomatocytes were used as control. Then the MCSs were carefully washed with cold PBS and observed with CLSM.

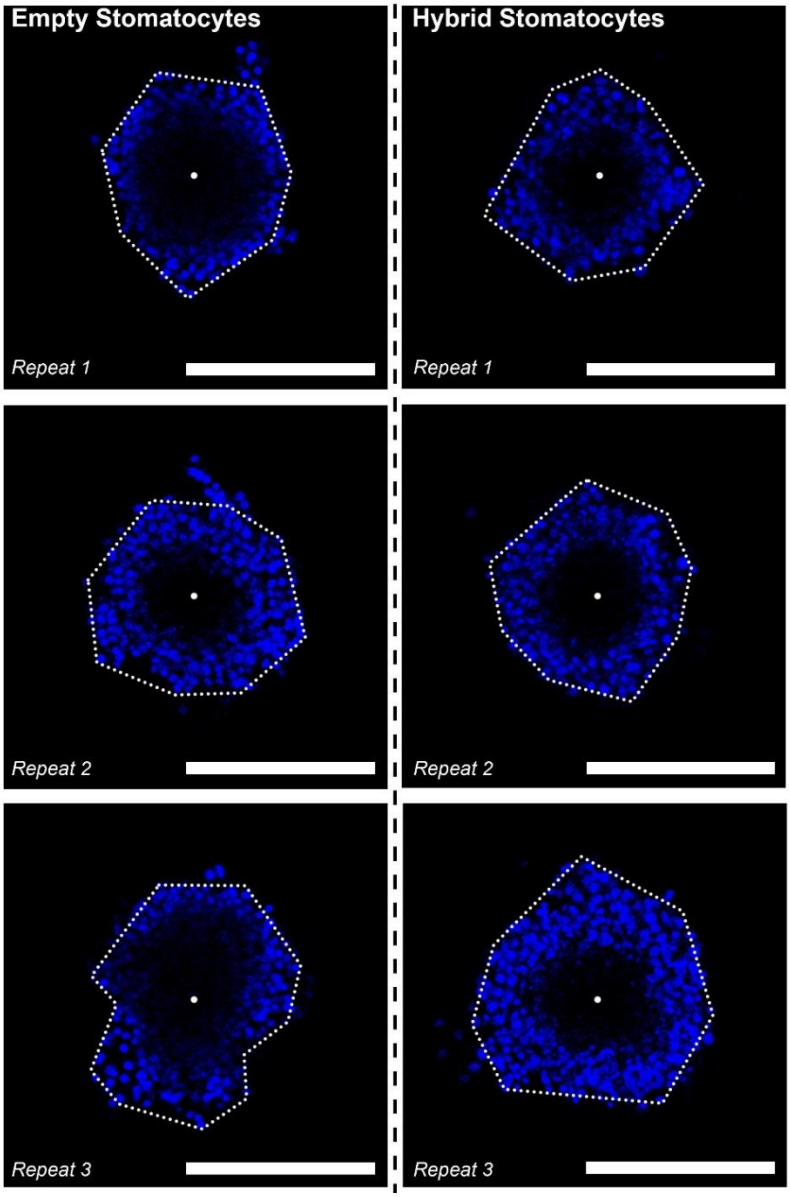

Figure S20. CLSM images for triplicate studies of particle penetration into 3D HeLa spheroids under the action of 250 µM H_2O_2. Here we used a nuclear stain (blue – Hoechst) to provide an indication of stability and overall morphology. Scale bars = 1 mm.

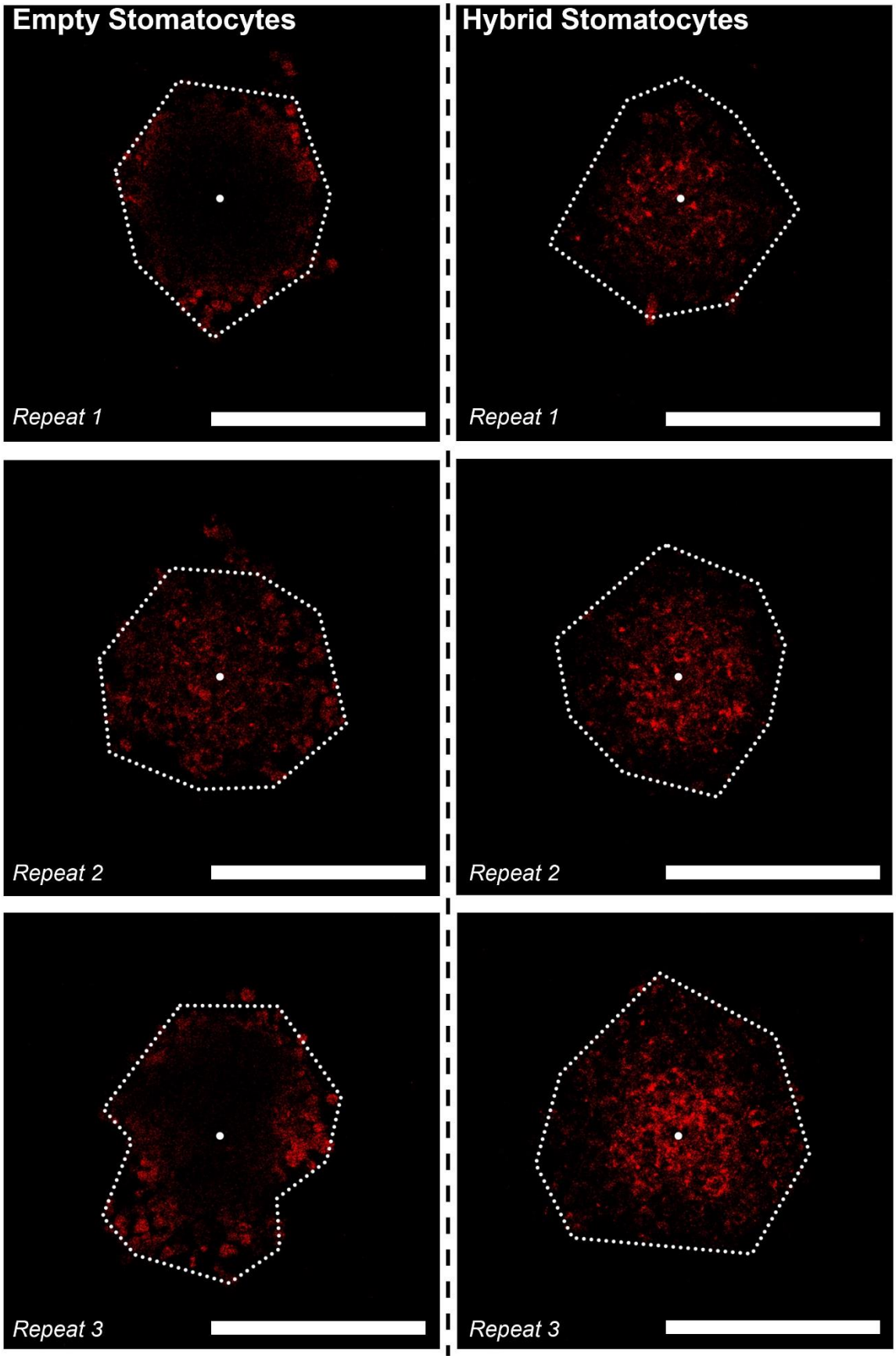

Figure S21. CLSM images for triplicate studies of particle penetration into 3D HeLa spheroids under the action of 250 µM H_2O_2 using a Cy5-labelled particles (red) to provide an indication of distribution. Images were taken at the widest point of the spheroids. Scale bars = 1 mm.

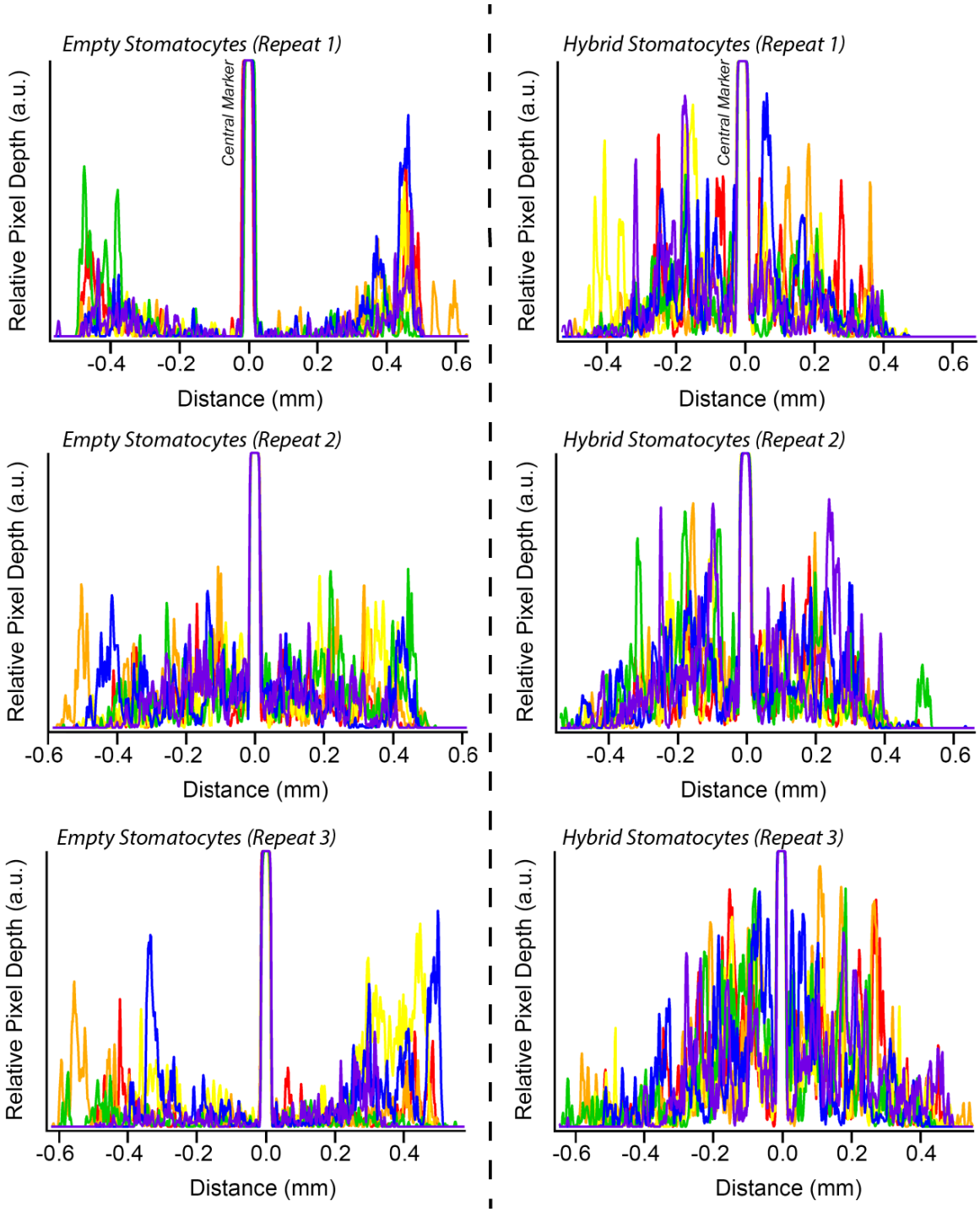

Figure S22. Line profiles extracted from CLSM images of particle penetration into 3D HeLa spheroids under the action of 250 µM H_2O_2 as presented in figure S21 - providing a qualitative demonstration that hybrid nanomotors outperform empty stomatocytes. Scale bars = 1 mm.

Supporting videos:

Video S1: Surface view from cryo-TEM tomography of MnP-loaded stomatocytes showing the overall structure of the nanomotor.
Video S2: Cryo-TEM tomography of MnP-loaded stomatocytes showing the structure of the MnO2 nanoparticles inside the cavity of the nanomotor.
Video S3: Compilation of NTA videos of motile MnP-loaded stomatocytes in the presence of fuel.
Video S4: NTA video of empty stomatocytes in the presence of fuel.
Video S5: NTA video of empty stomatocytes and free MnPs in the presence of fuel.

References

(1) Pijpers, I. A. B.; Abdelmohsen, L. K. E. A.; Williams, D. S.; Van Hest, J. C. M. Morphology under Control: Engineering Biodegradable Stomatocytes. *ACS Macro Lett.* **2017**, *6* (11), 1217–1222. https://doi.org/10.1021/acsmacrolett.7b00723.

(2) Abdelmohsen, L. K. E. A.; Williams, D. S.; Pille, J.; Ozel, S. G.; Rikken, R. S. M.; Wilson, D. A.; Van Hest, J. C. M. Formation of Well-Defined, Functional Nanotubes via Osmotically Induced Shape Transformation of Biodegradable Polymersomes. *J. Am. Chem. Soc.* **2016**, *138* (30), 9353–9356. https://doi.org/10.1021/jacs.6b03984.

(3) Jaganyi, D.; Altaf, M.; Wekesa, I. Synthesis and Characterization of Whisker-Shaped MnO2 Nanostructure at Room Temperature. *Appl. Nanosci.* **2013**, *3* (4), 329–333. https://doi.org/10.1007/s13204-012-0135-3.

(4) Mastronarde, D. N. Dual-Axis Tomography : An Approach with Alignment Methods That Preserve Resolution. *J. Struct. Biol.* **1997**, *120*, 343–352.

(5) Wilson, D. A.; Nolte, R. J. M.; van Hest, J. C. M. Autonomous Movement of Platinum-Loaded Stomatocytes. *Nat. Chem.* **2012**, *4* (4), 268–274. https://doi.org/10.1038/nchem.1281.

(6) Friedrich, J.; Seidel, C.; Ebner, R.; Kunz-Schughart, L. A. Spheroid-Based Drug Screen: Considerations and Practical Approach. *Nat. Protoc.* **2009**, *4* (3), 309–324. https://doi.org/10.1038/nprot.2008.226.

(7) Priwitaningrum, D. L.; Blondé, J. B. G.; Sridhar, A.; van Baarlen, J.; Hennink, W. E.; Storm, G.; Le Gac, S.; Prakash, J. Tumor Stroma-Containing 3D Spheroid Arrays: A Tool to Study Nanoparticle Penetration. *J. Control. Release* **2016**, *244*, 257–268. https://doi.org/10.1016/j.jconrel.2016.09.004.